Cellular/Molecular

Insufficient Oligodendrocyte Turnover in Optic Nerve Contributes to Age-Related Axon Loss and Visual Deficits

Jun-Jie Zhi,[1,2*] Shuang-Ling Wu,[2,3*] Hao-Qian Wu,[1,2*] Qi Ran,[1,2] Xing Gao,[2] Jing-Fei Chen,[2] Xing-Mei Gu,[2,4] Tao Li,[2] Fei Wang,[2] Lan Xiao,[2] Jian Ye,[1] and Feng Mei[2,3]

[1]Department of Ophthalmology and Institute of Surgery Research, Daping Hospital, Third Military Medical University (Army Medical University), Chongqing, 400042, China, [2]Department of Histology and Embryology, Chongqing Key Laboratory of Neurobiology, Brain and Intelligence Research Key Laboratory of Chongqing Education Commission, Third Military Medical University (Army Medical University), Chongqing, 400038, China, [3]School of Medicine, Chongqing University, Chongqing, 400030, China, and [4]Department of Medical English Teaching and Research, Third Military Medical University (Army Medical University), Chongqing, 400038, China

Age-related decline in visual functions is a prevalent health problem among elderly people, and no effective therapies are available up-to-date. Axon degeneration and myelin loss in optic nerves (ONs) are age-dependent and become evident in middle-aged (13-18 months) and old (20-22 months) mice of either sex compared with adult mice (3-8 months), accompanied by functional deficits. Oligodendrocyte (OL) turnover is actively going on in adult ONs. However, the longitudinal change and functional significance of OL turnover in aging ONs remain largely unknown. Here, using cell-lineage labeling and tracing, we reported that oligodendrogenesis displayed an age-dependent decrease in aging ONs. To understand whether active OL turnover is required for maintaining axons and visual function, we conditionally deleted the transcription factor Olig2 in the oligodendrocyte precursor cells of young mice. Genetically dampening OL turnover by Olig2 ablation resulted in accelerated axon loss and retinal degeneration, and subsequently impaired ON signal transmission, suggesting that OL turnover is an important mechanism to sustain axon survival and visual function. To test whether enhancing oligodendrogenesis can prevent age-related visual deficits, 12-month-old mice were treated with clemastine, a pro-myelination drug, or induced deletion of the muscarinic receptor 1 in oligodendrocyte precursor cells. The clemastine treatment or muscarinic receptor 1 deletion significantly increased new OL generation in the aged ONs and consequently preserved visual function and retinal integrity. Together, our data indicate that dynamic OL turnover in ONs is required for axon survival and visual function, and enhancing new OL generation represents a potential approach to reversing age-related declines of visual function.

Key words: **clemastine; myelin; myelination; oligodendrogenesis; OPC; RGC**

Significance Statement

Oligodendrocyte (OL) turnover has been reported in adult optic nerves (ONs), but the longitudinal change and functional significance of OL turnover during aging remain largely unknown. Using cell-lineage tracing and oligodendroglia-specific manipulation, this study reported that OL generation was active in adult ONs and the efficiency decreased in an age-dependent manner. Genetically dampening OL generation by Olig2 ablation resulted in significant axon loss and retinal degeneration, along with delayed visual signal transmission. Conversely, pro-myelination approaches significantly increased new myelin generation in aging ONs, and consequently preserved retinal integrity and visual function. Our findings indicate that promoting OL generation might be a promising strategy to preserve visual function from age-related decline.

Received Nov. 16, 2022; revised Jan. 16, 2023; accepted Jan. 27, 2023.

Author contributions: J.-J.Z., S.-L.W., H.-Q.W., Q.R., X.G., J.-F.C., T.L., F.W., and F.M. performed research; J.-J.Z., S.-L.W., H.-Q.W., Q.R., T.L., and F.W. analyzed data; H.-Q.W., X.-M.G., L.X., J.Y., and F.M. edited the paper; X.G., X.-M.G., T.L., L.X., and J.Y. contributed unpublished reagents/analytic tools; F.M. designed research; F.M. wrote the paper.

This work was supported by the STI 2030–Major Projects (2021ZD0201702), National Natural Science Foundation of China (82171417, 81901378, 32000723, 31921003), Chongqing Education Commission Fund (CXQT19009), and Young Elite Scientists Sponsorship Program by CAST (YESS 2019QNRC001). We thank Drs. J. Josh Lawrence (Texas Tech University) and Susumu Tonegawa (Massachusetts Institute of Technology) for the M1R floxed mice; Dr. Richard Lu (University of Cincinnati) for the Olig2 floxed mice; and Dr. Sonia Mayoral (Brown University) for critical reading of the manuscript.

*J.-J.Z., S.-L.W., and H.-Q.W. contributed equally to this work.

The authors declare no competing financial interests.

Correspondence should be addressed to Jian Ye at yejian1979@163.com or Feng Mei at meif@tmmu.edu.cn.

https://doi.org/10.1523/JNEUROSCI.2130-22.2023

Introduction

Age-related decline in visual functions emerges irreversibly in the elder population, such as impaired visual acuity and contrast sensitivity to visual signals (C. Zhang et al., 2008). The pathologic changes underlying the functional damages are complicated and remain elusive. The optic nerve (ON) is mainly made up of the axons of the retinal ganglion cells (RGCs) from the retina. The axons are susceptible to age and undergo irreversible degeneration with a ~40% decrease in axon number throughout the lifespan regardless of species (Cavallotti et al., 2002; Neufeld and Gachie, 2003; Harwerth et al., 2008; Calkins, 2013; Fortune et al.,

2014; Attia et al., 2019). For instance, the rate of axon loss is ~25% per year in mouse ONs, and the rate is ~0.5% (~5000 axons) annually in humans and rhesus monkeys (Mikelberg et al., 1989; Morrison et al., 1990; Neufeld and Gachie, 2003). Meanwhile, the retinal thickness displays an age-dependent decrease in the middle-aged and elderly population revealed by the optical coherence tomography (OCT) test (Cavallotti et al., 2004; C. Zhang et al., 2008; Patel et al., 2014; Lin et al., 2016). Unfortunately, effective therapies to slow down or reserve age-related axon loss and retinal degeneration are still unavailable in clinics so far.

The ON axons are nearly completely myelinated by mature oligodendrocytes (OLs) in adulthood (Skoff et al., 1976; Honjin et al., 1977; Bartsch et al., 1997; Dangata and Kaufman, 1997). Interestingly, newly generated OLs and myelin sheaths are continuously added to adult ONs from the differentiation of OL precursor cells (OPCs), indicating persistent OL turnover in adult ONs (Young et al., 2013; Hill et al., 2018). In addition, abnormalities of myelin sheaths have been repeatedly reported in the aged ONs of humans, nonhuman primates, and rodents (Sandell and Peters, 2001; Cavallotti et al., 2002; Attia et al., 2019), implying the involvement of OLs and myelin in the age-related pathologic changes of the visual system. In addition to ensuring the fast transmission of an action potential by myelin sheaths, recent studies have demonstrated that OLs can provide metabolic support for maintaining axonal integrity (Nave, 2010a,b; Simons and Nave, 2015; Chamberlain et al., 2021). However, it remains unclear how OL turnover contributes to the age-related changes of axons in ONs and visual functions.

In this study, we have shown that OL genesis is active in adult ONs but greatly diminished during aging, accompanied by axon loss and impaired visual function. Genetic inhibition of oligodendrogenesis in young mice by deleting transcriptional factor Olig2 in OPCs causes ON axon loss and latency delay of visual-evoked potentials (VEPs). Conversely, enhancing myelination by muscarinic receptor 1 (M1R) deletion or clemastine treatment promotes oligodendrogenesis in aging ONs, and consequently reverses axon loss and VEP latency delay. Together, our data indicate that dynamic OL turnover is required for RGC axon survival and visual function. Enhancing new OL generation may be a promising approach to reverse age-related visual function decline.

Materials and Methods

Animals. The C57BL/6J mice (WT) were purchased from the Laboratory Animal Center of the Third Military Medical University and Yangzhou Youdu Biotechnology. All transgenic mouse strains were maintained on a C57BL/6J background. The reporter gene mice, mT/mG line (The Jackson Laboratory, catalog #007676) or Tau-mGFP line (The Jackson Laboratory, catalog #021162) were crossed with the NG2-CreERT line (The Jackson Laboratory, catalog #008538) to obtain NG2-CreERT; Tau-mGFP and NG2-CreERT; mT/mG mice, respectively. The PLP-CreERT (The Jackson Laboratory, catalog #005795) was crossed with the mT/mG line to generate PLP-CreERT; mT/mG mice. The Olig2 floxed line and the M1R floxed line have been described previously (Young et al., 2013; F. Wang et al., 2018, 2020; J. F. Chen et al., 2021; L. Chen et al., 2021). The Olig2 floxed line was bred with the NG2-CreERT; Tau-mGFP line to generate NG2-CreERT; Tau-mGFP; Olig2 fl/fl mice and littermates (NG2-CreERT; Tau-mGFP; Olig2 fl/+). The M1R floxed line was crossed with NG2-CreERT; Tau-mGFP line to produce NG2-CreERT; Tau-mGFP; M1R fl/fl mice. Genotypes of all mice were determined using PCR analysis of tail genomic DNA with appropriate primers. Male and female mice were used for all experiments without bias. All animals were fed or bred in accordance with an approved protocol from the Laboratory Animal Welfare and Ethics Committee of Third Military Medical University.

Administration of tamoxifen. To induce Cre recombinase expression, tamoxifen (Sigma-Aldrich, catalog #T5648) was dissolved in corn oil at a concentration of 30 mg/ml and administered to the mice at 100 mg/kg per day for 4 consecutive days by oral gavage.

Drug treatment. The 12-month-old mice were treated with clemastine (SelleckChem, catalog #S1847) or an equivalent volume of vehicle. Clemastine was dissolved in DMSO at a concentration of 30 mg/ml and then diluted in drinking water. And the mice were proximately dosed at 10 mg/kg/day for 3 or 5 months continuously.

Frozen sections of ONs. Mice were deeply anesthetized with 1% pentobarbital and then were flushed with 0.01 M PBS, pH 7.2, transcardially, followed by 4% cold PFA in 0.1 M PB. ONs and retinas were collected for frozen sectioning and whole-mount preparation, respectively. ONs were postfixed in 4% PFA in 0.1 M PB overnight; then these tissues were dehydrated in 30% sucrose in 0.01 M PBS until submerged to the bottom. ONs were embedded in optimal cutting temperature compound (Sakura Finetek, 4583) and then sliced coronally or longitudinally at 10 μm equidistant intervals with a cryostat microtome (Cyrostar NX50, Fisher Scientific).

Immunofluorescence staining. For immunofluorescence staining, frozen sections were blocked with 5% BSA and 0.5% Triton X-100 for 2 h at room temperature, and then sequentially incubated with primary antibodies overnight at 4°C and the fluorescent dye-conjugated secondary antibodies for 2 h at room temperature. Primary antibodies included the following: rabbit anti-NG2 (1:500; Millipore, catalog #AB5320), rat anti-MBP (1:200; Millipore, catalog #MAB386), rabbit anti-NeuN (1:500; Abcam, catalog #ab177487), rabbit anti-Nav1.6 (1:1500; Alomone Labs, catalog #ASC-009), mouse anti-Caspr (1:1500; NeuoMab, catalog #75-001), mouse anti-CC1 (1:500; Calbiochem, catalog #OP80), goat anti-PDGFRα (1:500; R&D Systems, catalog #AF-1062), rabbit anti-neurofilament 200 (NF200) (1:500; Sigma-Aldrich, catalog #N4142), mouse anti-βIII-tubulin (1:200; Abcam, catalog #ab231084), mouse anti-Brn3a (1:500; Millipore, catalog #mab1585), and guinea pig anti-RNA-binding protein with multiple splicing (RBPMS) (1:300; Millipore, catalog #abn1376). Appropriate AlexaFluor-conjugated secondary antibodies included donkey anti-mouse, donkey anti-rabbit, donkey anti-goat, and donkey anti-rat (1:1000; Invitrogen). Nuclei were counterstained with DAPI at room temperature.

Whole-mount preparations of retina. The eyeballs were removed gently by microscissors and transferred to a tissue culture plate filled with 4% PFA immediately for 30 min at room temperature, and then placed in PBS under a dissecting microscope for retina isolation. A radial incision was made in the cornea, and the sclera was carefully dissected toward the ON with forceps. The cornea, sclera, ON, retina pigment epithelium, and lens were gently removed. Then, the retinal cup was cleaned, and hyaloid vessels were removed.

Flash VEPs (F-VEPs) test. Mice were anesthetized via intraperitoneal injection using a combination of xylazine (0.125 mg/kg) and ketamine (0.375 mg/kg) diluted in PBS. After dark adaptation for 5 min, the mice were fixed to the stereotaxic apparatus and VEP stimulation and recording began precisely 15 min after administration of anesthesia. One electrode was located at the primary visual cortexes as the active (positive) electrode, and another electrode was placed at the frontal cortex as the reference (negative) electrode. The ground electrode was placed at the base of the tail. The apparatus reduced interference from electrical noise (60 Hz) and heartbeat. The contralateral eye was covered by a lightproof patch while an eye was being tested. In each F-VEP experiment, 50 successive flash stimuli of 10 μs duration and 1 Hz frequency were delivered (intensity 120-200 mJ) (Firan et al., 2020; Cordano et al., 2022). According to the latencies, N1 was defined as the most reproducible negative peak between 30 and 60 ms and P1 as the most reproducible positive peak following N1 between 70 and 120 ms. For each VEP recording, we analyzed the latency and amplitude of N1/P1wave by referring to baseline (Mandel et al., 2013; Creel, 2019; Castoldi et al., 2020).

OCT test. The pupils were dilated using a 1% tropicamide solution. OCT image acquisition and analysis obtained by Heidelberg Spectralis and Bioptigen Envisu system averaged transverse scan images were used as a measure of retinal thickness (Galetta et al., 2011; X. Zhang et al.,

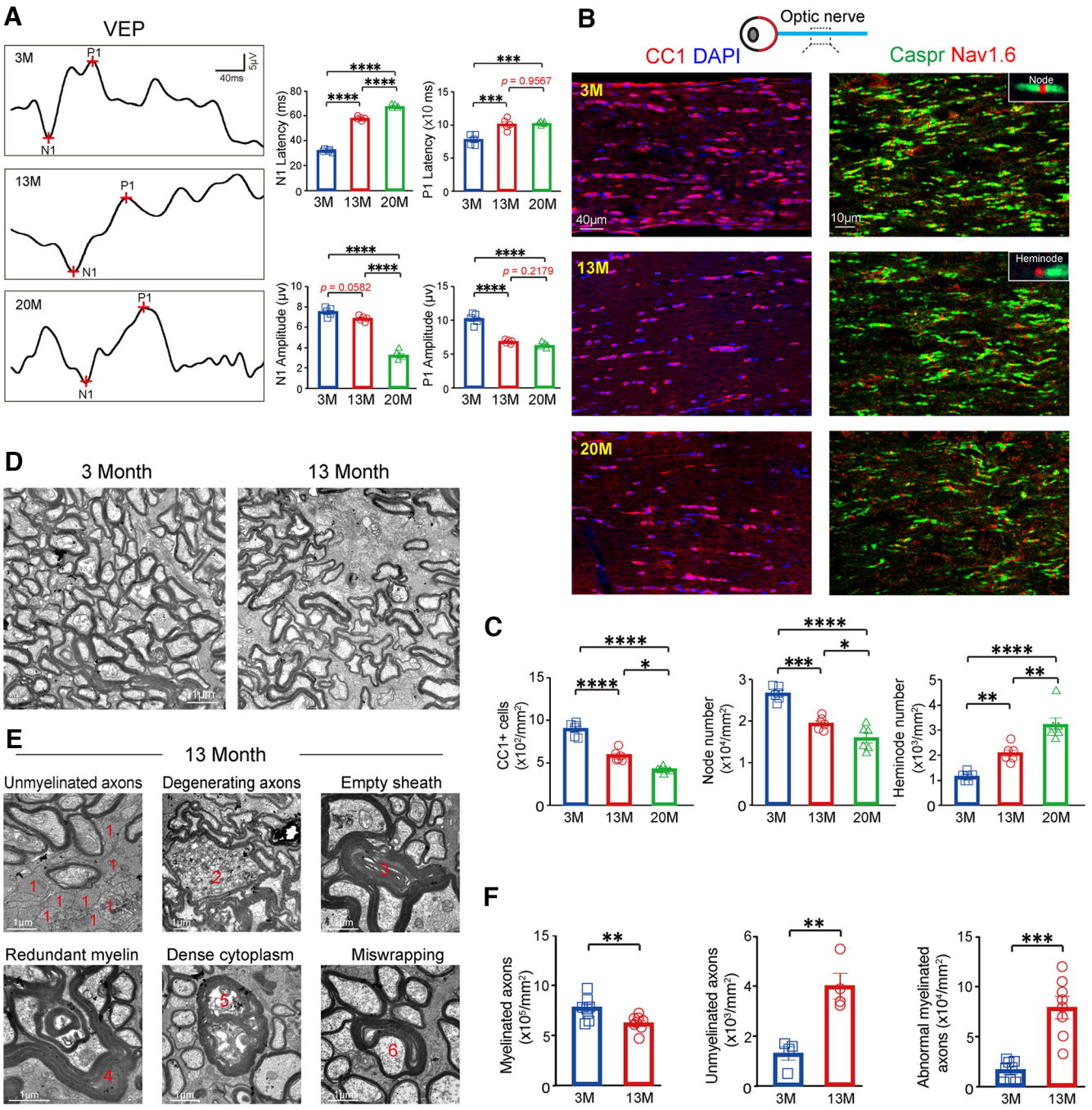

Figure 1. Age-related functional decline and myelin loss in ONs. ***A***, Waveforms of VEP and quantification of wave latencies and amplitudes of N1 and P1 components in 3-, 13-, and 20-month-old mice. $n = 5$ (3 month), 9 (13 month), and 13 (20 month) mice. Error bars indicate mean ± SEM. ***$p < 0.005$; ****$p < 0.0001$; multiple comparisons of ANOVA. ***B***, Representative images showing CC1$^+$ OL (red, left panels) and Nav1.6$^+$ nodal (green) and Caspr$^+$ (red) paranodal regions (right panels) on the longitudinal sections of ONs at the age of 3, 13, and 20 months. Insets: top, node; bottom, heminode. Scale bars: left panels, 40 μm; right panels, 10 μm. ***C***, Numbers of CC1$^+$ cells and Nav1.6$^+$/Caspr$^+$ nodes/heminodes were quantified in the ONs, respectively. $n = 4$ or 5 mice in each group. Error bars indicate mean ± SEM. *$p < 0.05$; **$p < 0.01$; ***$p < 0.005$; ****$p < 0.0001$; multiple comparisons of ANOVA. ***D–F***, Representative EM images of 3-month and 13-month ONs (***D***). Numbers indicate unmyelinated axons (1), degenerating axon (2), empty sheath (3), redundant myelin (4), dense cytoplasm (5), and miswrapping myelin (6) in 13-month-old ONs (***E***). Myelinated, unmyelinated, and abnormal axons were quantified (***F***). Scale bar, 1 μm. $n = 8$ ONs in each group. Error bars indicate mean ± SEM. **$p < 0.01$; ***$p < 0.005$; *t* test.

2019). To minimize the time for scanning, we chose to scan four areas of each eye (1.2 mm from the optic disk in both vertical and horizontal directions). The average of the four measurements was considered to be the retinal thickness of each eye. The inner retinal layer (IRL, the combination of the retinal nerve fiber layer and the ganglion cell plus the inner plexiform layer) thickness was measured to assess retinal degeneration.

Electron microscope. For electron microscopy, ONs were dissected after transcardial perfusion and postfixed with 4% PFA and 2% glutaraldehyde in cacodylate buffer for at least a week at 4°C. The tissue was osmicated, dehydrated, and embedded in Epon resin. Semithin (1 μm) or ultrathin (90 nm) sections of the ON were stained with lead citrate. Micrographs were acquired using a JEM-1400 electron microscope with a Gatan camera. The myelinated fibers were calculated using ImageJ software.

Image acquisition and quantification. Fluorescent images were captured using a confocal laser-scanning microscope (Olympus, FV 3000) or a spinning disk confocal super-resolution microscope (Olympus, SpinSR10) with excitation wavelengths appropriate for AlexaFluor-488

(488 nm), -594 (568 nm), or -647 (628 nm) or DAPI (380 nm). For the statistical analysis, at least seven images were recorded from each ON. At least four areas of each eye (1.2 mm from the optic disk in vertical and horizontal directions) were recorded on the retina. Quantification was performed using Image-Pro Plus 5 (Media Cybernetics).

Statistical analysis. All graph data are presented as mean ± SEM, and points represent individual animals. Mice were randomly assigned to different time points or treatments. Two-tailed unpaired *t* test or one-way ANOVA followed by Bonferroni's test was used to determine the statistical difference between the normally distributed data. Significance and nonsignificant *p* values are reported in the figures.

Results

Age-related OL and myelin loss in ONs

To understand age-related changes in visual functions, we set out to use the VEP test on mature adult (3-8 months), middle-aged (13-18 months), and old (20-22 months) mice (Fig. 1*A*). Upon visual stimuli, electric signals were recorded from the visual cortex accordingly (Creel, 2019). The latency of the VEP waves mirrors the transmission speed in the optical system (Iliescu et al., 2018). The waves were reproducible in adult healthy controls (data not shown). We found that the latencies of both N1 and P1 waves were significantly delayed in the 13-month-old mice compared with the 3-month-old mice, and the N1 wave was further prolonged in the 20-month-old mice (Fig. 1*A*). Meanwhile, the amplitude of N1 or P1 wave was also dramatically decreased at an advanced age (20 months) compared with the mature adults (3 months) or the middle-aged mice (13 months) (Fig. 1*A*), reflecting inhibited excitability of the visual pathway in the old mice. These results manifest an age-related decline in visual function.

The VEP latency is considered as a sensitive biomarker for myelin changes in the visual system, and the extent of latency delay is closely associated with the degree of myelin loss in the ONs of demyelinating animal models (Mozafari et al., 2010; Farley et al., 2019; Heidari et al., 2019; Cordano et al., 2022). We reasoned that the decreased latency in the middle-aged and old mice may be attributed to oligodendroglia and myelin impairment. Thus, we assessed the changes in oligodendroglia and myelin in ONs at different ages (Fig. 1*B–F*). As expected, the $CC1^+$ mature OL density exhibited an age-dependent decrease in the middle-aged and the old ONs compared with the mature adult mice (Fig. 1*B*,*C*). In support of this finding, the number of nodes of Ranvier revealed by immunostaining for Caspr (a paranodal marker) and sodium channel 1.6 (Nav1.6, a nodal marker) was significantly decreased in the middle-aged mice in contrast to the adult mice and was further declined in the old mice accompanied with a higher density of heminodes (Fig. 1*B*,*C*). Under transmission electron microscopy, the axons were almost fully myelinated in the 3-month-old ONs and the myelinated axon density was significantly decreased in the 13-month-old mice (Fig. 1*D*,*F*). In addition, unmyelinated axons and abnormal myelinated axons, including empty sheaths, redundant myelin, dense cytoplasm, and miswrapping, were more frequently seen in the 13-month-old ONs (Fig. 1*E*,*F*), in contrast to the 3-month-old ONs. These results indicate age-related OL and myelin loss in ONs.

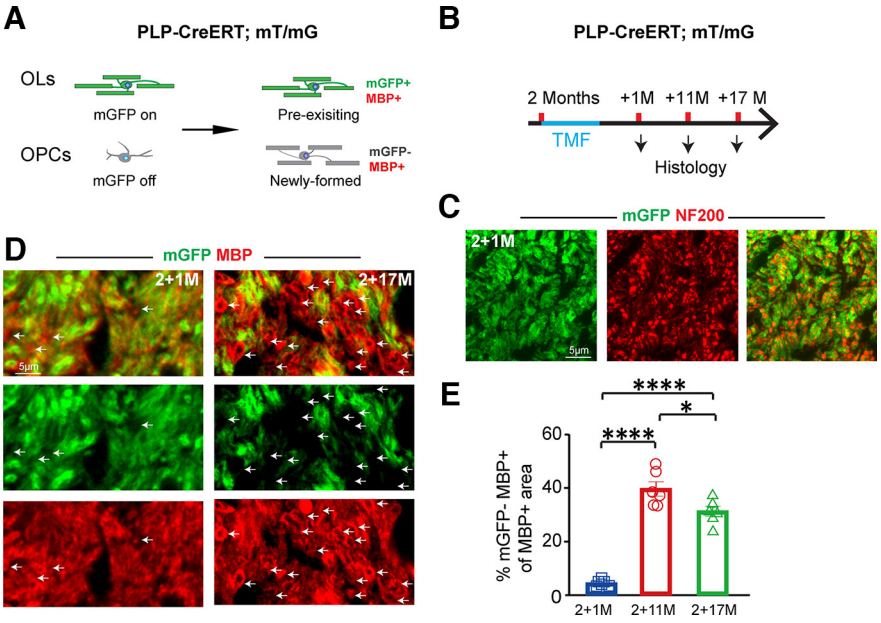

Figure 2. OL turnover in ONs during aging. ***A***, ***B***, Schematic diagram represents mGFP expression by preexisting OLs ($MBP^+/mGFP^+$) but not by newly generated OLs from OPC differentiation ($MBP^+/mGFP^-$) after induction (***A***) and the time course of tamoxifen induction and histology examination in the PLP-CreERT; mT/mG mice (***B***). ***C***, Representative images of $mGFP^+$ myelin (green) and NF200-positive axons (red) on cross-sections of ONs at 2 + 1 months after induction. Scale bar, 5 μm. ***D***, Representative images of mGFP (green) and MBP (red) positive myelin in ONs 2 + 1 and 2 + 17 months after induction. Arrows indicate $MBP^+/mGFP^-$ myelin. Scale bar, 5 μm. ***E***, Quantifications of the $mGFP^+/MBP^+$ percentage myelin in 2 + 1-, 2 + 11-, and 2 + 17-month-old ONs. $n = 6$ mice in each group. Error bars indicate mean ± SEM. $^*p < 0.05$; $^{****}p < 0.0001$; multiple comparisons of ANOVA.

Ratio of OL turnover in adult ONs

Given the age-related loss of OLs and myelin, we sought to understand the dynamic change of myelin during aging. OLs are a type of terminal cell, and the preexisting OLs can be replaced by newly generated OLs from OPC differentiation, when preexisting OLs undergo cell death (Baumann and Pham-Dinh, 2001; Young et al., 2013; Stadelmann et al., 2019). Numerous studies have well-documented continuous new OL addition in adult brain and ONs (Young et al., 2013; Hill et al., 2018; Hughes et al., 2018; Yang et al., 2020), but the ratio of myelin replacement in ONs remains unclear during aging. Thus, we sought to assess the ratio of OL turnover by labeling preexisting OLs and associated myelin sheaths in the PLP-CreERT; mT(omato)/mG(FP) mice (Fig. 2*A*). Technically, the preexisting OLs start to express membrane-bounded GFP (mGFP) on induction, and the MBP and mGFP double-positive ($MBP^+/mGFP^+$) structures are the myelin sheaths generated by preexisting OLs (Fig. 2*A*). Because the Cre recombinase is not expressed by OPCs, the newly added OLs from OPC differentiation after induction do not express mGFP, and can be identified as the $MBP^+/mGFP^-$ area (Fig. 2*A*). The 2-month-old PLP-CreERT; mT/mG mice were induced by tamoxifen, and the mice were killed at the age of 2 + 1, 2 + 11, or 2 + 17 months for histology examination (Fig. 2*B*). Nearly all the NF200-positive axons were closely associated with the $mGFP^+$ structures on the cross sections of ONs (Fig. 2*C*). Indeed, ~95% MBP^+ area was also $mGFP^+$ in the 2 + 1-month ONs, indicating a high recombination rate driven by the PLP-CreERT (Fig. 2*D*,*E*). Remarkably, ~38% MBP^+ area was $mGFP^-$ in the 2 + 11-month ONs, suggesting that ~33% of myelin was newly generated within

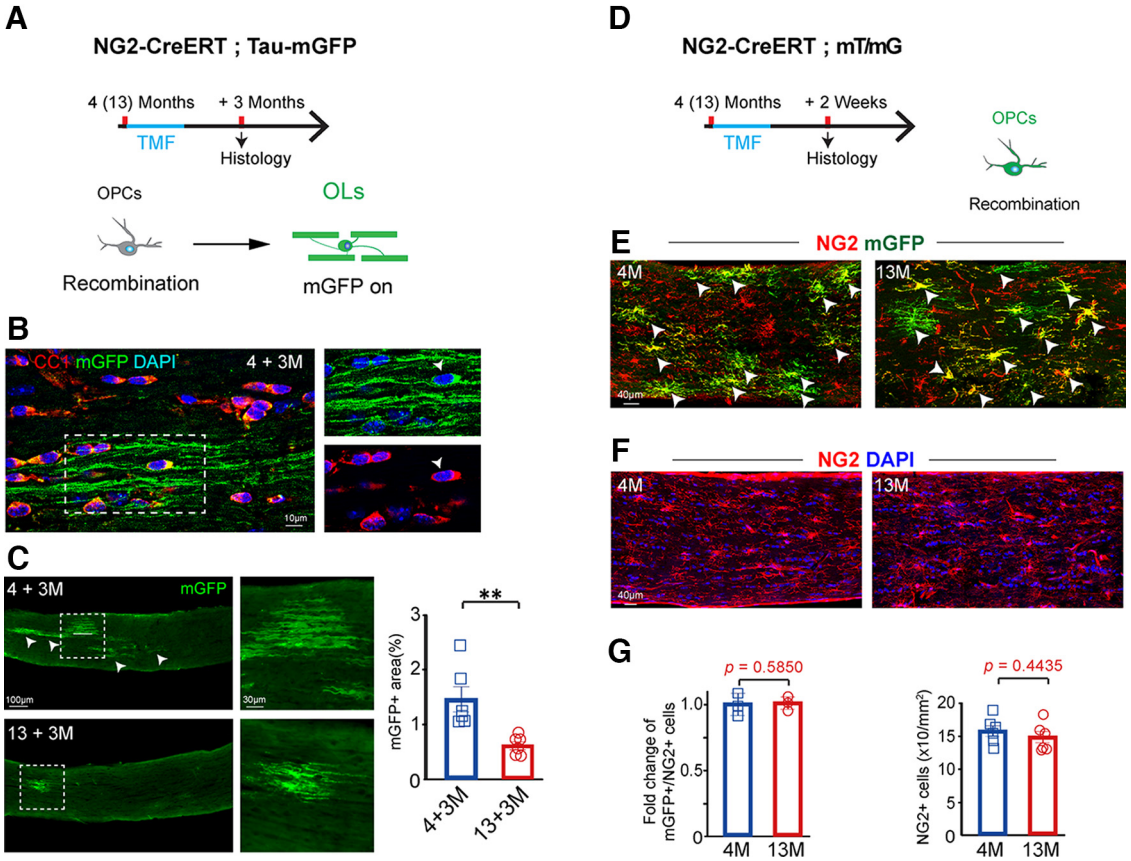

Figure 3. Age-dependent decline of oligodendrogenesis in ONs. ***A***, Schematic diagram represents the time course of tamoxifen induction and histology examination, and mGFP expression in the NG2-CreERT; Tau-mGFP mice. ***B***, Representative images of $mGFP^+$ cells (green, arrowhead) express CC1 (red) in the 4 + 3-month-old ONs. Right panels are enlarged images. Scale bar, 10 μm. ***C***, Representative images and quantifications of $mGFP^+$ new myelin in the ONs 3 months after induction at the age of 4 or 13 months. $n = 6$ mice in each group. Areas of $mGFP^+$ myelin sheaths were quantified. Scale bars: left panels, 100 μm; right panels, 30 μm. Data are mean ± SEM. $^{**}p < 0.01$ (*t* test). ***D***, ***E***, Schematic diagram represents the time course of tamoxifen induction and histology examination, and recombination in OPCs (***D***). Representative images of mGFP/NG2 double-positive cells (arrowheads) in the 4- and 13-month-old ONs (***E***). $n = 3$ mice in each group. Scale bar, 40 μm. ***F***, Representative images of $NG2^+$ OPCs on the longitudinal sections of ONs at the age of 4 and 13 months. Scale bar, 40 μm. ***G***, Fold change of mGFP/NG2 double-positive cells (left) and $NG2^+$ cell number (right) were quantified. Left, $n = 3$ mice in each group for the $mGFP^+/NG2^+$ cell number. Right, $n = 5$-8 mice in each group for the number of $NG2^+$ cells. Error bars indicate mean ± SEM (*t* test).

10 months compared with the 2 + 1-month ONs (5% $mGFP^-$ area) (Fig. 2*D*,*E*), and this result implies that OL turnover is actively going on in adult ONs. Interestingly, the ratio was slightly decreased to ~31% at the age of 2 + 17 months (Fig. 2*E*). Since this ratio change may attribute to a number of factors in a complicated manner, including the survival rate of axons and myelin, and the speed of new myelin generation, the exact mechanisms underlying the ratio change remain undetermined. Regarding that the capacity of OPCs to differentiate into mature OLs declines steeply in aging brains, it is plausible that oligodendrogenesis may contribute to the rate of OL/myelin turnover during aging (Neumann et al., 2019; Segel et al., 2019; Iram et al., 2022).

Diminished oligodendrogenesis in aging ONs

To understand whether oligodendrogenesis is changed in aging ONs, we used the NG2-CreERT; Tau-mGFP mice to label newly formed OLs and associated myelin sheaths (Fig. 3*A*,*B*). Because the expression of mGFP is under the control of the Tau promoter, newly formed myelin sheaths and OLs can be visualized for highly expressing Tau (mGFP) (Fig. 3*A*,*B*), while the OPCs are $mGFP^-$ for a very low level of Tau expression (Young et al., 2013; McKenzie et al., 2014; Xiao et al., 2016; F. Wang et al., 2020; J. F. Chen et al., 2021). The 4- and 13-month-old mice were induced by tamoxifen and were killed 3 months later. A large amount of mGFP-expressing myelin sheaths was visualized in the 4 + 3-month-old ONs; in contrast, new myelin was greatly diminished in the 13 + 3-month ONs (Fig. 3*B*,*C*). To exclude the possibility that the recombination efficiency was altered by age, we crossed the NG2-CreERT line with the mT/mG line. Upon recombination, the $NG2^+$ cells started to express mGFP in the NG2-CreERT; mT/mG ONs (Fig. 3*D*). The recombination efficiency was examined 2 weeks after induction by counting the ratio of $mGFP^+$ cells in $NG2^+$ OPCs. Our results showed a similar recombination rate between the 4- and 13-month-old ONs (Fig. 3*E*,*G*), suggesting that age does not alter recombination efficiency. In addition, the $NG2^+$ OPC density was not significantly different between the 4- and 13-month-old ONs (Fig. 3*F*,*G*), indicating that the diminished oligodendrogenesis is because of inhibited differentiation but not insufficiency of OPCs during aging.

Age-related axon loss and retinal thinning

Since OLs play a crucial role for maintaining axon integrity, we next wanted to know how the ON axons are affected by age. Immunostaining for NF200 on cross sections of ONs revealed that the axon density was evidently decreased in the 13-month-old ONs compared with the 3-month-old ONs, and it was further declined at the age of 20 months (Fig. 4*A*). Notably, the

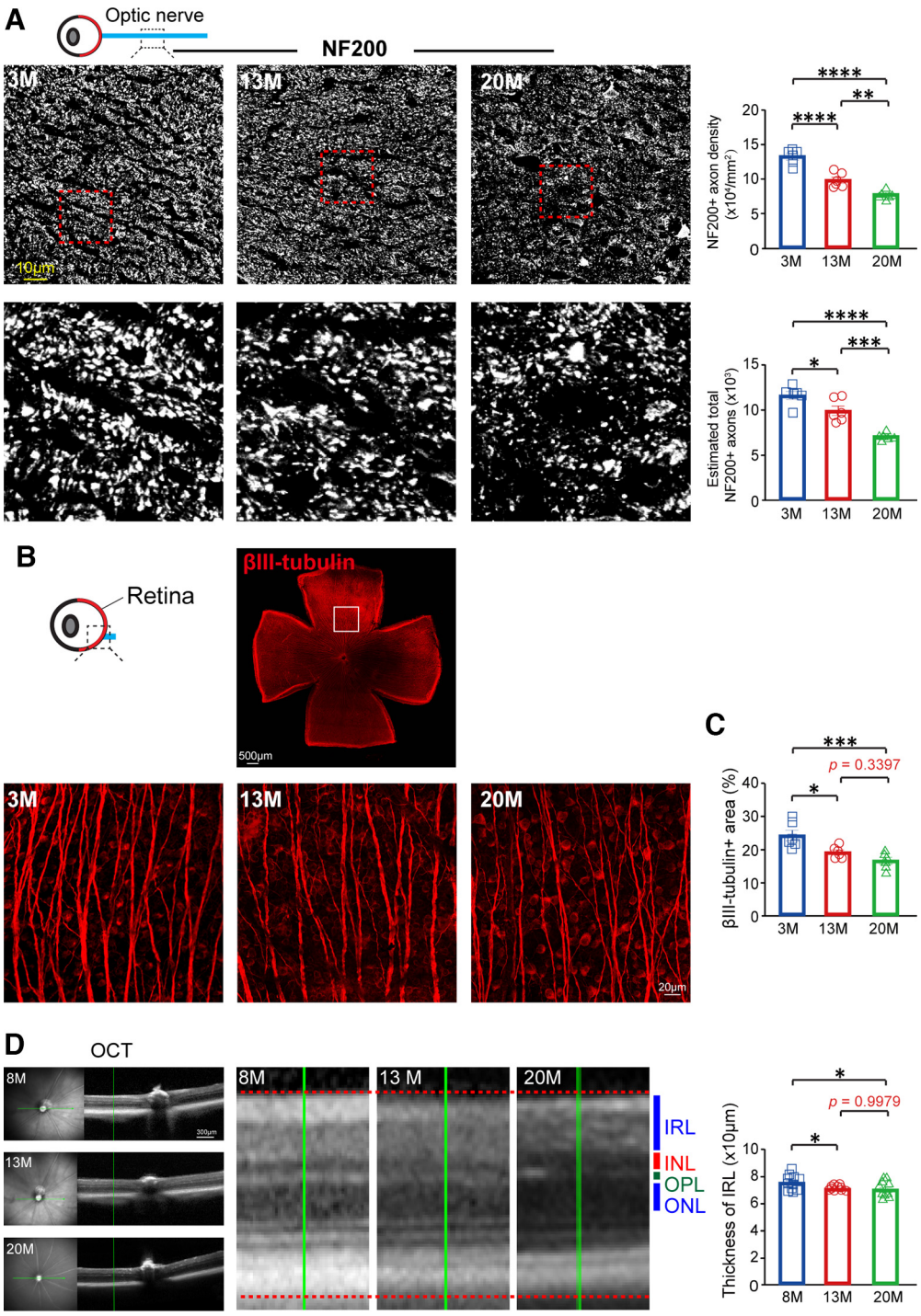

Figure 4. Age-related RGC axon loss and retinal degeneration in aging ONs. ***A***, Representative images and quantification of NF200-positive axons on cross-sections of ONs at the age of 3, 13, and 20 months. Bottom panels correspond to the boxes in the top panels. $n = 5$ or 6 mice in each group. Scale bar, 10 μm. Error bars indicate mean ± SEM. *$p < 0.05$; **$p < 0.01$; ***$p < 0.005$; ****$p < 0.0001$; multiple comparisons of ANOVA. ***B***, ***C***, Representative images (***B***) and quantifications (***C***) of βIII-tubulin (red) positive RGC axons, respectively, on whole-mount preparations at the age of 3, 13, and 20 months. Left panels, Boxes represent the sampling regions. $n = 6$-9 mice in each group. Scale bars: left panels, 500 μm; middle and right panels, 20 μm. $n = 5$-9 mice in each group. Data are mean ± SEM. *$p < 0.05$; ***$p < 0.005$; multiple comparisons of ANOVA. ***D***, Representative images of OCT showing the retina and quantification of the thickness of IRL at the age of 8, 13, and 20 months. INL, Inner nuclear layer; OPL, outer plexiform layer; ONL, outer nuclear layer. $n = 9$-11 mice in each group. Scale bar, 300 μm. Error bars indicate mean ± SEM. *$p < 0.05$; multiple comparisons of ANOVA.

estimated total number of axons in the ONs decreased by ~15% in the 13-month-old ONs followed by a steep decline of axon number by ~40% in the 20-month-old ONs compared with the 3-month-old ONs, respectively (Fig. 4*A*), indicating progressive and massive axon loss in ONs during aging (Sandell and Peters, 2001; Cavallotti et al., 2002; Calkins, 2013).

Since all the axons in ONs are projected from the RGCs of the retina, we wanted to understand the changes of RGC axons in the retina. To assess RGC axon density, we conducted immunostaining for βIII-tubulin on whole-mount preparations of the retinas at different ages (Fig. 4*B*). Consistently, our results indicate that the βIII-tubulin$^+$ area was significantly decreased in

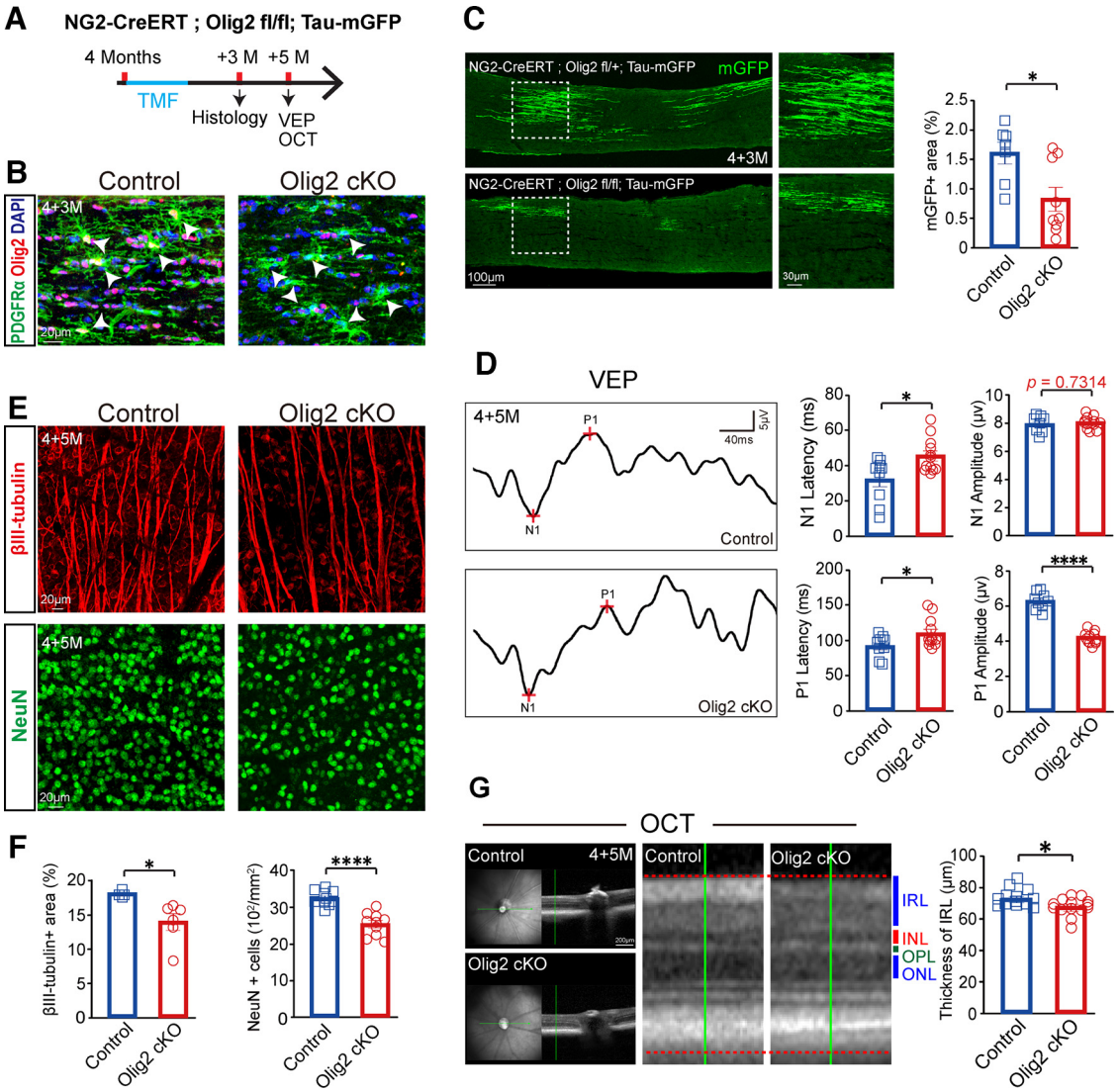

Figure 5. RGC axon loss and functional deficits in Olig2 cKO ONs. ***A***, Schematic diagram represents the time course of tamoxifen induction, histology, OCT, and VEP. ***B***, Representative images showing Olig2 expression (red) in PDGFRα^+ OPCs (green, arrows) of the control and Olig2 cKO ONs. Scale bar, 20 μm. ***C***, Confocal images and quantification of mGFP$^+$ cells and myelin sheaths on longitudinal sections of controls and Olig2 cKO ONs. Areas of mGFP$^+$ myelin sheaths in each group were quantified. Scale bars: left panels, 100 μm; right panels, 30 μm. $n = 7$-9 mice in each group. Data are mean ± SEM. *$p < 0.05$ (*t* test). ***D***, Waveforms of VEP and quantification of wave latencies and amplitudes of N1 and P1 in control and Olig2 cKO mice. $n =$ 9-12 mice for each group. Error bars indicate mean ± SEM. *$p < 0.05$; ****$p < 0.0001$ (two-tailed unpaired *t* test). ***E***, Representative images of βIII-tubulin (red, top panels) positive RGC axons and NeuN$^+$ (green, bottom panels) RGC neurons (Extended Data Fig. 5-1) on whole-mount preparations of control and Olig2 cKO eyes. Scale bar, 20 μm. ***F***, Quantification of the βIII-tubulin$^+$ area and NeuN$^+$ number in retina. $n = 7$-9 mice in each group. Error bars indicate mean ± SEM. *$p < 0.05$. ****$p < 0.0001$. ***G***, Representative images of OCT showing the retina and quantification the thickness of IRL in control and Olig2 cKO mice 5 months after induction at the age of 4 months. $n = 10$ or 11 mice in each group. Scale bar, 200 μm. Error bars indicate mean ± SEM. *$p < 0.05$ (two-tailed unpaired *t* test).

the 13-month-old retina in contrast to the 3-month-old retina, although there was no significant change between 13-month-old mice and 20-month-old mice (Fig. 4*C*). This indicates age-dependent loss of RGC axons in the retina and ONs. The retina is a multiple-layer nervous structure that is responsible for translating light into neuronal impulses (Eliasieh et al., 2007; Sugita et al., 2020). To understand whether retina undergoes degeneration during aging, we next measured the IRL (the combination of the retinal nerve fiber layer and the ganglion cell plus the inner plexiform layer) thickness using OCT (Fig. 4*D*) (Cruz-Herranz et al., 2019). OCT is a noninvasive and noncontact method to give a cross-sectional image of the retina (Podoleanu, 2012; Theelen and Teussink, 2018). In line with these findings, our results demonstrated a significant decrease in IRL thickness in the middle-aged mice compared with the adult mice, while no significant change was found between the old and middle-aged IRL (Fig. 4*D*) (Hsu et al., 2012; Fortune et al., 2014; Jorge et al., 2019). These results indicate massive RGC axon loss and evident retinal degeneration during aging.

New OL generation is required for axon survival and retinal integrity

Given the coincidence of declining OL genesis and axon loss, we hypothesized that OL turnover is required for axonal and retinal integrity. To test this possibility, we induced Olig2 deletion specifically in the PDGFRα^+ OPCs of the NG2-CreERT; Olig2 fl/fl; Tau-mGFP line (Fig. 5*A*,*B*). Olig2 is a transcriptional factor that is selectively expressed by oligodendroglia and essential for OPC differentiation (Zhou et al., 2001; Mei et al., 2013; Yu et al., 2013; F. Wang et al., 2020). As expected, the mGFP$^+$ new myelin was

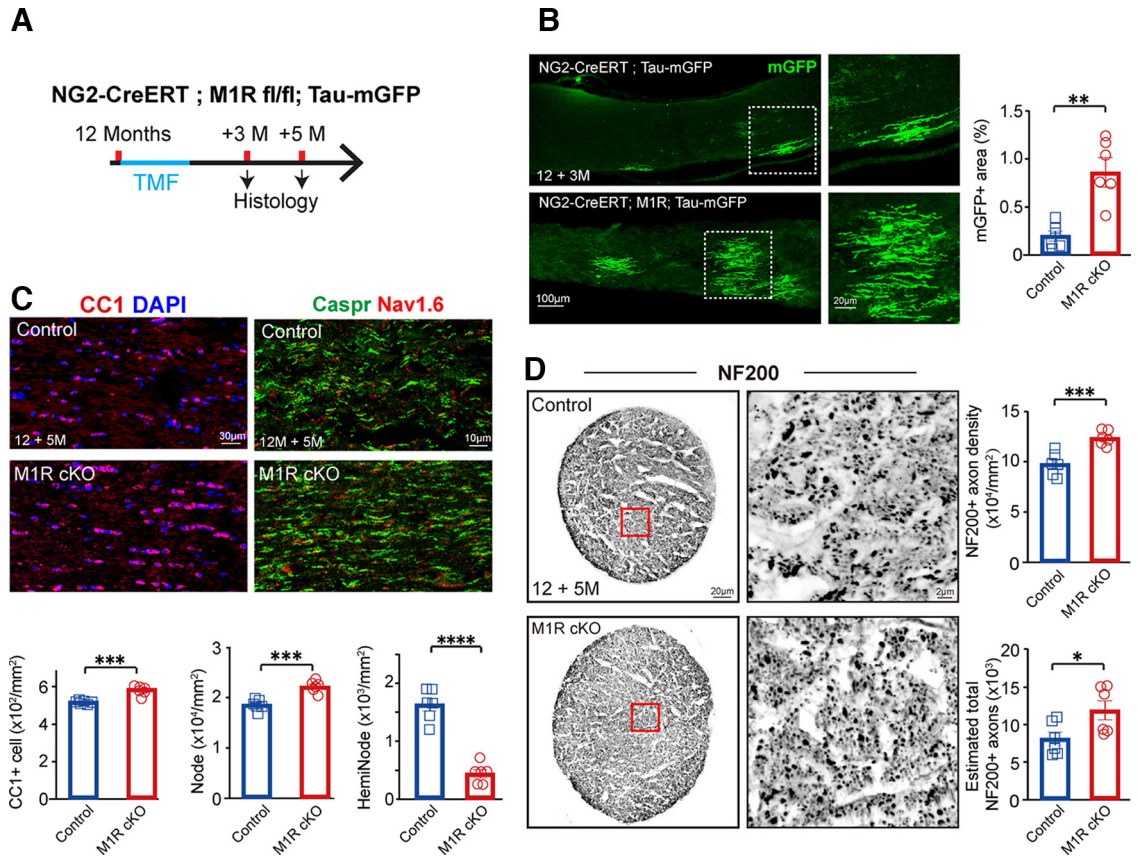

Figure 6. Enhanced oligodendrogenesis preserves axons from age-related degeneration in M1R cKO ONs. ***A***, Schematic diagram represents the time course of tamoxifen induction and histology. ***B***, Confocal images and quantification of mGFP$^+$ cells and myelin sheaths on longitudinal sections of control and M1R cKO ONs. Scale bars: left panels, 100 μm; right panels, 20 μm. $n = 6$ mice in each group. Data are mean ± SEM. $^{**}p < 0.01$; $^{****}p < 0.0001$ (*t* test). ***C***, Representative images and quantifications of CC1$^+$ OL (red, left panels), and Nav1.6(green)/Caspr (red) positive nodes/heminodes (right panels) on the longitudinal sections of the control and M1R cKO ONs 5 months after induction at the age of 12 months. $n = 10$-12 mice in each group. Scale bars: left panels, 30 μm; right panels, 10 μm. Error bars indicate mean ± SEM. $^{***}p < 0.005$; $^{****}p < 0.0001$ (*t* test). ***D***, Representative images and quantification of NF200-positive axons on cross-sections of the control and M1R cKO ONs 5 months after induction at the age of 12 months; the right panels are corresponding to the boxes in the left panels. $n = 6$ mice in each group. Scale bars: left panels, 20 μm; right panels, 2 μm. Error bars indicate mean ± SEM. $^{*}p < 0.05$; $^{***}p < 0.005$; *t* test.

significantly decreased in the Olig2 cKO ONs compared with the age-matched controls (Olig2 heterozygotes), 3 months after induction of recombination at the age of 4 months (Fig. 5*C*). Therefore, the Olig2 cKO mice are suitable to model insufficient OL turnover in aging ONs and assess whether active OL turnover is required for the structural and functional integrity of the visual system (Fig. 5*D*,*E*). The VEP test manifested that the latencies of both N1 and P1 waves were significantly prolonged in the Olig2 cKO mice 5 months after induction compared with the controls, and the P1 amplitude was significantly inhibited (Fig. 5*D*). Thus, inhibiting OL turnover resulted in decreased signal transmission of the visual system. This is probably because of decreased myelinogenesis induced by Olig2 deletion. We next asked whether OL turnover is required for RGC axon survival. We examined the neuronal and axonal densities by immunostaining for NeuN and βIII-tubulin on the whole-mount preparations of retina, respectively (Fig. 5*E*). Interestingly, the densities of NeuN$^+$ neurons and βIII-tubulin$^+$ axons were significantly decreased in the Olig2 cKO retina compared with the controls (Fig. 5*F*). The majority of NeuN$^+$ neurons are RGC bodies, since >90% of NeuN$^+$ cells coexpress Brn3a and RBPMS, two specific RGC markers (Extended Data Fig. 5-1). These results indicate that active OL turnover is required for RGC axon survival in the retina. In support of these findings, we found that the thickness of IRL was significantly decreased in the Olig2 cKO mice compared with the controls revealed by OCT (Fig. 5*G*). Therefore, it is evident that active OL turnover is required for axon integrity and insufficient OL turnover contributes, at least partially, to age-related functional deficits.

Enhancing OL turnover preserves axons from age-related degeneration

Since active OL turnover is required for RGC axon integrity and visual function, we next wanted to examine whether enhancing oligodendrogenesis can rescue age-related axon degeneration in ONs. Previously, we have identified M1R as a negative regulator for OPC differentiation, and OPC-specific deletion of M1R accelerates myelinogenesis in aged and neurodegenerative brains (Mei et al., 2016; F. Wang et al., 2018; J. F. Chen et al., 2021). Thus, we induced conditional deletion of M1R in the 12-month-old NG2-CreERT; M1R fl/fl; Tau-mGFP mice, and examined whether silencing M1R signaling in OPCs can promote oligodendrogenesis in the aging ONs (Fig. 6*A*). Excitingly, the M1R deletion driven by NG2-CreERT resulted in increased mGFP$^+$ myelin 3 months after induction, indicating that M1R deletion is sufficient to enhance oligodendrogenesis in the aging ONs (Fig. 6*B*). In support of these findings, the M1R deletion in OPCs resulted in a significant increase of CC1$^+$ OL density and Caspr$^+$/Nav1.6$^+$ node number in the M1R cKO ONs compared with the age-matched controls, along with a decreased heminode density (Fig. 6*C*). These results demonstrate that M1R antagonism

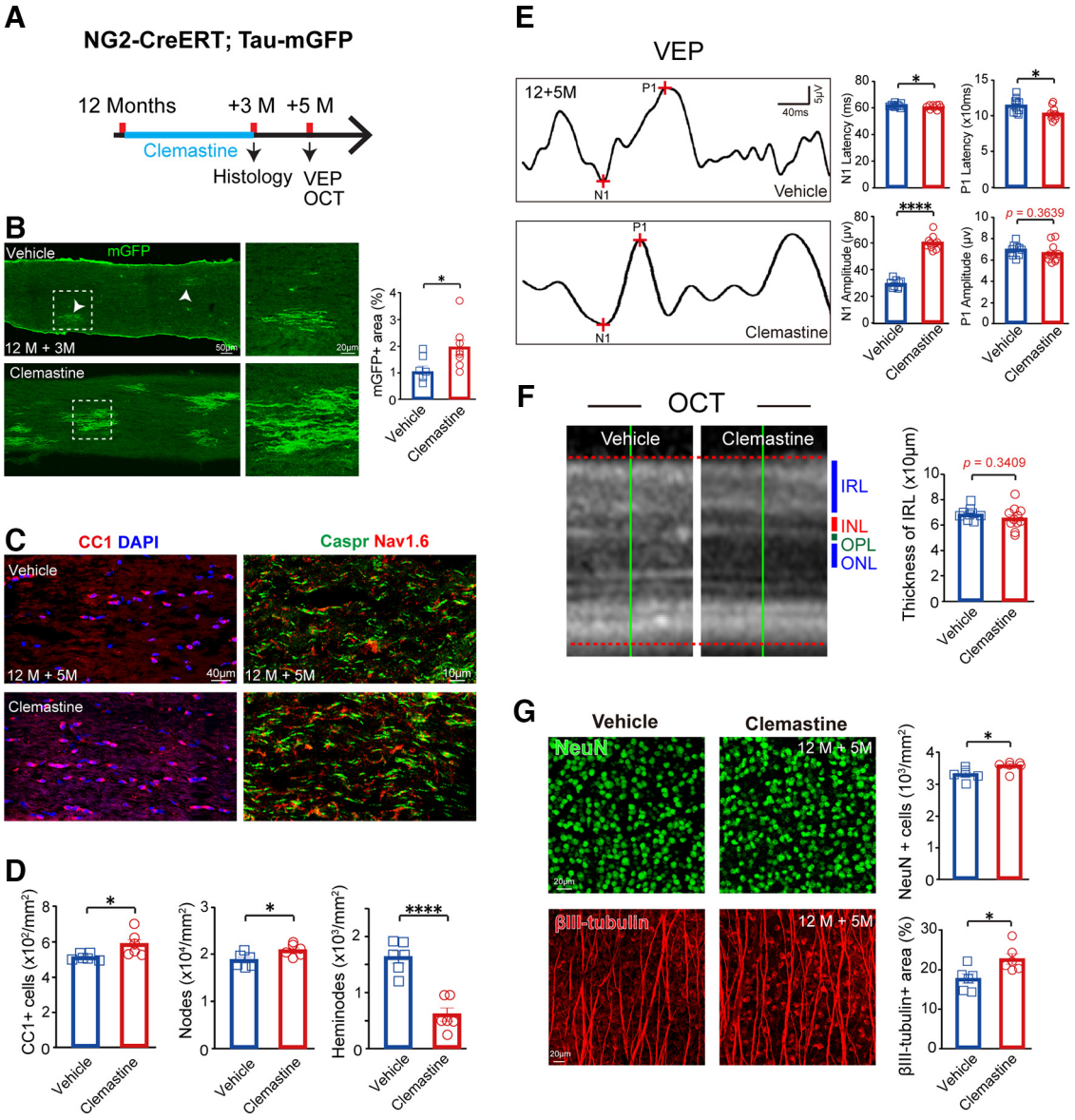

Figure 7. Clemastine rescues age-related retinal degeneration and functional deficits. ***A***, Schematic diagram represents the time course of tamoxifen induction, clemastine treatment, histology, OCT, and VEP. ***B***, Confocal images and quantification of mGFP$^+$ cells and myelin sheaths on longitudinal sections of the vehicle or clemastine-treated ONs. $n = 7$ or 8 mice in each group. Scale bars: left panels, 50 μm; right panels, 20 μm. Data are mean ± SEM. *$p < 0.05$ (*t* test). ***C***, ***D***, Representative images of CC1$^+$ OL and Nav1.6 (green)/Caspr (red) positive node and heminodes on the longitudinal sections of the vehicle and clemastine-treated ONs (***C***), and quantifications of OL number, node, and heminode densities (***D***). $n = 6$ mice in each group. Scale bars: left panels, 40 μm; right panels, 10 μm. Error bars indicate mean ± SEM. *$p < 0.05$; ****$p < 0.0001$ (*t* test). ***E***, Waveforms of VEP and quantitation of P1 wave latency in vehicle and clemastine-treated mice. $n = 14$-19 mice for each group. Error bars indicate mean ± SEM. *$p < 0.05$; ****$p < 0.0001$ (*t* test). ***F***, Representative images and quantification of the thickness of IRL in vehicle and clemastine-treated mice by OCT. $n = 14$-19 mice for each group. Error bars indicate mean ± SEM. Significance is based on two-tailed unpaired *t* test. ***G***, Representative images and quantifications of NeuN (green) and βIII-tubulin (red) positive RGC neurons and axons on whole-mount preparations of eyes treated with vehicle or clemastine. Scale bar, 20 μm. $n = 10$-13 mice in each group. Error bars indicate mean ± SEM. *$p < 0.05$ (*t* test).

can rejuvenate endogenous oligodendrogenesis and promote myelin regeneration in aging ONs. Then, we assessed axon density on cross-sections by immunostaining for NF200, and our results indicated that axon density was significantly increased in the M1R cKO ONs compared with the age-matched controls (Fig. 6*D*). These results demonstrate that silencing M1R signaling enhances oligodendrogenesis and consequently preserves axons from age-related degeneration in ONs.

Clemastine treatment reverses age-related RGC axon loss and visual deficits

Since muscarinic antagonism is effective to rejuvenate oligodendrogenesis in aging ONs, we next assessed whether clemastine, an FDA-approved anticholinergic drug, can promote OL turnover, and preserve retinal integrity and visual function (Fig. 7*A*). To confirm that clemastine can improve oligodendrogenesis in aging ONs, we treated the 12-month NG2-CreERT; Tau-mGFP mice with clemastine or vehicle for 3 months after induction (Fig. 7*A*). As expected, the mGFP$^+$ myelin was significantly increased by the clemastine treatment compared with the vehicle-treated mice (Fig. 7*B*). As a result, the CC1$^+$ mature OL density and the number of nodes were both increased remarkably in the clemastine-treated 12 + 5-month-old ONs with a decrease of heminodal density in contrast to the vehicle-treated mice (Fig. 7*C*,*D*). These results indicate that clemastine is effective in promoting OL turnover. Strikingly, the VEP test revealed that both N1 and P1 latency were significantly shortened with dramatically elevated N1 amplitude, in the 12 + 5-month-old mice treated with clemastine (Fig. 7*E*),

suggesting that clemastine can reverse age-related visual function decline. To examine the retinal integrity, the retinas were examined by OCT, and our result manifested that the IRL thickness was not significantly changed in the clemastine-treated mice compared with the vehicle-treated controls (Fig. 7*F*), while the neuron and axon densities in the retina were better preserved compared with the vehicle-treated mice, revealed by immunostaining for NeuN and βIII-tubulin, respectively, on whole-mount preparations (Fig. 7*G*). These results indicate that clemastine treatment promotes oligodendrogenesis, and consequently protects RGC axons and visual functions from age-related degradation.

Together, our results demonstrate that OL turnover is required for axonal integrity and visual function. Enhancing OL turnover by pro-myelination approaches can rescue age-related axon loss and function deficits (Fig. 8).

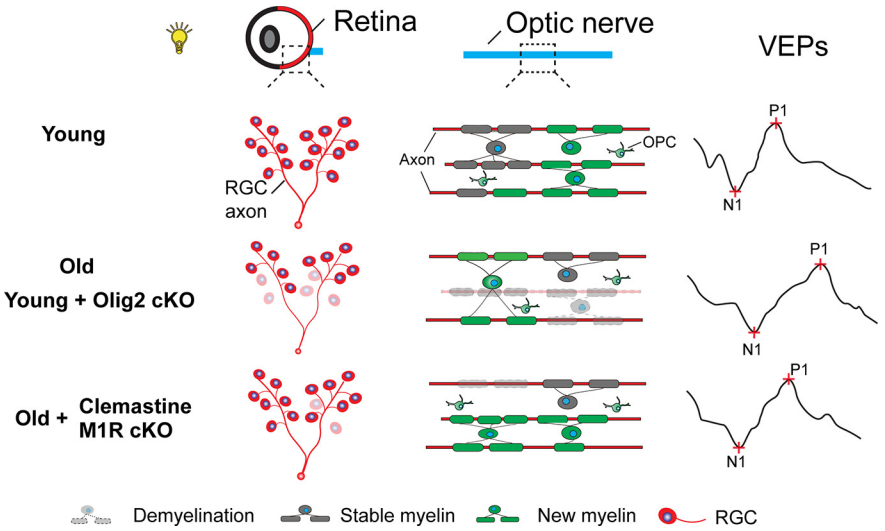

Figure 8. Graphic abstract showing that enhancing OL turnover is effective to rescue age-related retinal degeneration and visual function declines.

Discussion

The ON axons are sensitive to age and undergo degeneration inevitably during aging (Cavallotti et al., 2004; Eliasieh et al., 2007; Samuel et al., 2011; Patel et al., 2014). Thus, it becomes an unmet need to develop effective approaches to slow down axon degeneration and preserve visual function. The RGC axons are almost completely myelinated in ONs (Skoff et al., 1976; Honjin et al., 1977; Bartsch et al., 1997; Dangata and Kaufman, 1997), and noticeably adult-born OLs are continuously added to ONs to replace preexisting OLs (Young et al., 2013; Yang et al., 2020). In this study, we have shown that active OL turnover is required for preserving axon density and visual function and the efficiency is declined evidently in aged ONs. Increasing oligodendrogenesis by M1R antagonism can protect RGC axons from age-related degeneration and preserve visual functions in aged mice. Together, our findings indicate promoting endogenous oligodendrogenesis as a potential approach to reverse age-related visual deficits.

Myelin sheaths are comparably stable once formed and undergo degeneration slowly in adult brains (Young et al., 2013; Yeung et al., 2014; Tripathi et al., 2017; Hill et al., 2018). It has been demonstrated that >90% of myelin can survive for >18 months in mouse corpus callosum by tracing sparsely labeled preexisting myelin (Tripathi et al., 2017; Hill et al., 2018). Similarly, our previous study estimated ~10% of preexisting myelin in the layer I to III of the mouse cortex undergo degeneration within 10 months (F. Wang et al., 2020). Notably, the degenerative rate of preexisting OL is much higher in ONs, it is estimated that ~30% OLs undergo degeneration within 12 months (Tripathi et al., 2017). Consistent with this finding, our results indicate that ~38% of preexisting myelin was replaced by new myelin in ONs within 11 months. These findings suggest that the degenerative rate of myelin is region-dependent, although the underlying mechanisms remain undefined. Previous studies have demonstrated OLs are heterogeneous in the adult and neurodegenerative brains (Marques et al., 2016; Foerster et al., 2019; Jäkel et al., 2019; Sadick et al., 2022). It is possible that the heterogeneity of OLs may contribute to the variable susceptibility to age.

Active OL turnover has been reported previously by using either BrdU/EdU incorporation or cell-lineage labeling and tracing (Kang et al., 2010; Hughes et al., 2013; Baxi et al., 2017; Hill et al., 2018). OL turnover is an important mechanism to replace apoptotic OLs and degenerating myelin sheaths (Hughes et al., 2013). As OPCs are capable of differentiating into mature OLs and generating myelin sheaths throughout the lifetime, the persistent existing OPCs become a convenient precursor reservoir for OL turnover in ONs (Young et al., 2013; Tripathi et al., 2017; Yang et al., 2020). It is important to note that a large number of axons remain unmyelinated and partially myelinated in adult brains, allowing for intercalating new myelin sheaths (Baumann and Pham-Dinh, 2001; Foerster et al., 2019; Stadelmann et al., 2019; Chapman and Hill, 2020). Previous studies have demonstrated that new OL generation in adult brains is required for adapting to new environments, new skill learning, and memory consolidation (McKenzie et al., 2014; Xiao et al., 2016; Hughes et al., 2018; Pan et al., 2020; Steadman et al., 2020). In contrast, >95% of axons are myelinated in adult ONs; thus, the newly formed OLs are presumably to replace apoptotic OLs. Noticeably, the OL turnover rate decreases significantly in the ONs and brains older than 13 months because of insufficient OPC differentiation in aging CNS (F. Wang et al., 2020).

Regarding the coincidence of myelin loss and axon degeneration in aging ONs, we report that OL turnover is an important mechanism to sustain RGC axon integrity and visual function. Olig2 is a transcriptional factor that is important for OPC differentiation but not required for OL survival or axon integrity (Zhou et al., 2001; Mei et al., 2013). Genetically dampening OPC differentiation leads to RGC axon loss and visual impairments, suggesting that active oligodendrogenesis is required for retinal integrity and visual functions. Recent studies have shown that OLs are essential for maintaining axonal integrity by providing metabolic support for axons (Nave, 2010a,b). For example, OLs fuel axons by transporting lactates and SIRT2 (Nave, 2010a; Chamberlain et al., 2021). It remains unclear why ON axons are nearly fully myelinated and whether it is related to the demand of energy. Nevertheless, it is important to note that OL turnover in adult ONs is essential to preserve RGC axons from

degeneration. Thus, the impaired visual functions are attributed, at least partially, to the declining OL turnover in aged mice.

The endogenous abilities to generate new OLs steeply decline in aged ONs and brains. The mechanisms that dampen OPC differentiation during aging remain elusive, and overactivated inhibitory signals and declining capacities to differentiate have been implicated (Ruckh et al., 2012; Young et al., 2013; Neumann et al., 2019; Segel et al., 2019; Rivera et al., 2021). One possible strategy to overcome the inhibitory mechanisms is to enhance endogenous myelination through pro-myelination approaches. M1R has been identified previously as a negative regulator for OPC differentiation, and the M1R antagonism is effective in promoting myelinogenesis in the aged and neurodegenerative brains (Mei et al., 2014, 2016; F. Wang et al., 2018, 2020; L. Chen et al., 2021). We found that M1R deletion in OPCs can promote OL generation in aging ONs, and more importantly, preserve axon density from declining. In support with this notion, we found that clemastine can promote OL turnover in aged ONs and subsequently rescue visual impairments. Clemastine is an FDA-approved drug with antimuscarinic properties and is powerful in promoting myelinogenesis in multiple sclerosis patients (Green et al., 2017). Our results imply that pro-myelination therapies as a potential approach to protect visual function from age-related decline.

Reference

Attia H, Taha M, Abdellatif A (2019) Effects of aging on the myelination of the optic nerve in rats. Int J Neurosci 129:320–324.

Bartsch S, Montag D, Schachner M, Bartsch U (1997) Increased number of unmyelinated axons in optic nerves of adult mice deficient in the myelin-associated glycoprotein (MAG). Brain Res 762:231–234.

Baumann N, Pham-Dinh D (2001) Biology of oligodendrocyte and myelin in the mammalian central nervous system. Physiol Rev 81:871–927.

Baxi EG, DeBruin J, Jin J, Strasburger HJ, Smith MD, Orthmann-Murphy JL, Schott JT, Fairchild AN, Bergles DE, Calabresi PA (2017) Lineage tracing reveals dynamic changes in oligodendrocyte precursor cells following cuprizone-induced demyelination. Glia 65:2087–2098.

Calkins DJ (2013) Age-related changes in the visual pathways: blame it on the axon. Invest Ophthalmol Vis Sci 54:Orsf37–41.

Castoldi V, Marenna S, d'Isa R, Huang SC, De Battista D, Chirizzi C, Chaabane L, Kumar D, Boschert U, Comi G, Leocani L (2020) Non-invasive visual evoked potentials to assess optic nerve involvement in the dark agouti rat model of experimental autoimmune encephalomyelitis induced by myelin oligodendrocyte glycoprotein. Brain Pathol 30:137–150.

Cavallotti C, Pacella E, Pescosolido N, Tranquilli-Leali FM, Feher J (2002) Age-related changes in the human optic nerve. Can J Ophthalmol 37:389–394.

Cavallotti C, Artico M, Pescosolido N, Leali FM, Feher J (2004) Age-related changes in the human retina. Can J Ophthalmol 39:61–68.

Chamberlain KA, Huang N, Xie Y, LiCausi F, Li S, Li Y, Sheng ZH (2021) Oligodendrocytes enhance axonal energy metabolism by deacetylation of mitochondrial proteins through transcellular delivery of SIRT2. Neuron 109:3456–3472.e8.

Cruz-Herranz A, Dietrich M, Hilla AM, Yiu HH, Levin MH, Hecker C, Issberner A, Hallenberger A, Cordano C, Lehmann-Horn K, Balk LJ, Aktas O, Ingwersen J, von Gall C, Hartung HP, Zamvil SS, Fischer D, Albrecht P, Green AJ (2019) Monitoring retinal changes with optical coherence tomography predicts neuronal loss in experimental autoimmune encephalomyelitis. J Neuroinflammation 16:203.

Chapman TW, Hill RA (2020) Myelin plasticity in adulthood and aging. Neurosci Lett 715:134645.

Chen JF, Liu K, Hu B, Li RR, Xin W, Chen H, Wang F, Chen L, Li RX, Ren SY, Xiao L, Chan JR, Mei F (2021) Enhancing myelin renewal reverses cognitive dysfunction in a murine model of Alzheimer's disease. Neuron 109:2292–2307.e5.

Chen L, Ren SY, Li RX, Liu K, Chen JF, Yang YJ, Deng YB, Wang HZ, Xiao L, Mei F, Wang F (2021) Chronic exposure to hypoxia inhibits myelinogenesis and causes motor coordination deficits in adult mice. Neurosci Bull 37:1397–1411.

Cordano C, Sin JH, Timmons G, Yiu HH, Stebbins K, Guglielmetti C, Cruz-Herranz A, Xin W, Lorrain D, Chan JR, Green AJ (2022) Validating visual evoked potentials as a preclinical, quantitative biomarker for remyelination efficacy. Brain 145:3943–3952.

Creel DJ (2019) Visually evoked potentials. Handb Clin Neurol 160:501–522.

Dangata YY, Kaufman MH (1997) Myelinogenesis in the optic nerve of (C57BL × CBA) F1 hybrid mice: a morphometric analysis. Eur J Morphol 35:3–17.

Eliasieh K, Liets LC, Chalupa LM (2007) Cellular reorganization in the human retina during normal aging. Invest Ophthalmol Vis Sci 48:2824–2830.

Farley BJ, Morozova E, Dion J, Wang B, Harvey BD, Gianni D, Wipke B, Cadavid D, Wittmann M, Hajos M (2019) Evoked potentials as a translatable biomarker to track functional remyelination. Mol Cell Neurosci 99:103393.

Firan AM, Istrate S, Iancu R, Tudosescu R, Ciuluvică R, Voinea L (2020) Visual evoked potential in the early diagnosis of glaucoma: literature review. Rom J Ophthalmol 64:15–20.

Foerster S, Hill MF, Franklin RJ (2019) Diversity in the oligodendrocyte lineage: plasticity or heterogeneity? Glia 67:1797–1805.

Fortune B, Reynaud J, Cull G, Burgoyne CF, Wang L (2014) The effect of age on optic nerve axon counts, SDOCT scan quality, and peripapillary retinal nerve fiber layer thickness measurements in rhesus monkeys. Transl Vis Sci Technol 3:2.

Galetta KM, Calabresi PA, Frohman EM, Balcer LJ (2011) Optical coherence tomography (OCT): imaging the visual pathway as a model for neurodegeneration. Neurotherapeutics 8:117–132.

Green AJ, Gelfand JM, Cree BA, Bevan C, Boscardin WJ, Mei F, Inman J, Arnow S, Devereux M, Abounasr A, Nobuta H, Zhu A, Friessen M, Gerona R, von Budingen HC, Henry RG, Hauser SL, Chan JR (2017) Clemastine fumarate as a remyelinating therapy for multiple sclerosis (ReBUILD): a randomised, controlled, double-blind, crossover trial. Lancet 390:2481–2489.

Harwerth RS, Wheat JL, Rangaswamy NV (2008) Age-related losses of retinal ganglion cells and axons. Invest Ophthalmol Vis Sci 49:4437–4443.

Heidari M, Radcliff AB, McLellan GJ, Ver Hoeve JN, Chan K, Kiland JA, Keuler NS, August BK, Sebo D, Field AS, Duncan ID (2019) Evoked potentials as a biomarker of remyelination. Proc Natl Acad Sci USA 116:27074–27083.

Hill RA, Li AM, Grutzendler J (2018) Lifelong cortical myelin plasticity and age-related degeneration in the live mammalian brain. Nat Neurosci 21:683–695.

Honjin R, Sakato S, Yamashita T (1977) Electron microscopy of the mouse optic nerve: a quantitative study of the total optic nerve fibers. Arch Histol Jpn 40:321–332.

Hsu SY, Ko ML, Linn G, Chang MS, Sheu MM, Tsai RK (2012) Effects of age and disc area on optical coherence tomography measurements and analysis of correlations between optic nerve head and retinal nerve fibre layer. Clin Exp Optom 95:427–431.

Hughes EG, Kang SH, Fukaya M, Bergles DE (2013) Oligodendrocyte progenitors balance growth with self-repulsion to achieve homeostasis in the adult brain. Nat Neurosci 16:668–676.

Hughes EG, Orthmann-Murphy JL, Langseth AJ, Bergles DE (2018) Myelin remodeling through experience-dependent oligodendrogenesis in the adult somatosensory cortex. Nat Neurosci 21:696–706.

Iliescu DA, Ciubotaru A, Ghiţă MA, Păun AM, Ion T, Zăgrean L (2018) Electrophysiologic evaluation of the visual pathway at different depths of sevoflurane anesthesia in diabetic rats. Rom J Ophthalmol 62:34–41.

Iram T, et al. (2022) Young CSF restores oligodendrogenesis and memory in aged mice via Fgf17. Nature 605:509–515.

Jäkel S, Agirre E, Mendanha Falcão A, van Bruggen D, Lee KW, Knuesel I, Malhotra D, Ffrench-Constant C, Williams A, Castelo-Branco G (2019) Altered human oligodendrocyte heterogeneity in multiple sclerosis. Nature 566:543–547.

Jorge L, Canário N, Quental H, Bernardes R, Castelo-Branco M (2019) Is the retina a mirror of the aging brain? Aging of neural retina layers and primary visual cortex across the lifespan. Front Aging Neurosci 11:360.

Kang SH, Fukaya M, Yang JK, Rothstein JD, Bergles DE (2010) $NG2^+$ CNS glial progenitors remain committed to the oligodendrocyte lineage in postnatal life and following neurodegeneration. Neuron 68:668–681.

Lin HC, Tew TB, Hsieh YT, Lin SY, Chang HW, Hu FR, Chen WL (2016) Using optical coherence tomography to assess the role of age and region in corneal epithelium and palisades of vogt. Medicine (Baltimore) 95: e4234.

Mandel Y, Goetz G, Lavinsky D, Huie P, Mathieson K, Wang L, Kamins T, Galambos L, Manivanh R, Harris J, Palanker D (2013) Cortical responses elicited by photovoltaic subretinal prostheses exhibit similarities to visually evoked potentials. Nat Commun 4:1980.

Marques S, et al. (2016) Oligodendrocyte heterogeneity in the mouse juvenile and adult central nervous system. Science 352:1326–1329.

McKenzie IA, Ohayon D, Li H, de Faria JP, Emery B, Tohyama K, Richardson WD (2014) Motor skill learning requires active central myelination. Science 346:318–322.

Mei F, Wang H, Liu S, Niu J, Wang L, He Y, Etxeberria A, Chan JR, Xiao L (2013) Stage-specific deletion of Olig2 conveys opposing functions on differentiation and maturation of oligodendrocytes. J Neurosci 33:8454–8462.

Mei F, Fancy SP, Shen YA, Niu J, Zhao C, Presley B, Miao E, Lee S, Mayoral SR, Redmond SA, Etxeberria A, Xiao L, Franklin RJ, Green A, Hauser SL, Chan JR (2014) Micropillar arrays as a high-throughput screening platform for therapeutics in multiple sclerosis. Nat Med 20:954–960.

Mei F, Lehmann-Horn K, Shen YA, Rankin KA, Stebbins KJ, Lorrain DS, Pekarek K, Sagan SA, Xiao L, Teuscher C, von Budingen HC, Wess J, Lawrence JJ, Green AJ, Fancy SP, Zamvil SS, Chan JR (2016) Accelerated remyelination during inflammatory demyelination prevents axonal loss and improves functional recovery. Elife 5:e18246.

Mikelberg FS, Drance SM, Schulzer M, Yidegiligne HM, Weis MM (1989) The normal human optic nerve: axon count and axon diameter distribution. Ophthalmology 96:1325–1328.

Morrison JC, Cork LC, Dunkelberger GR, Brown A, Quigley HA (1990) Aging changes of the rhesus monkey optic nerve. Invest Ophthalmol Vis Sci 31:1623–1627.

Mozafari S, Sherafat MA, Javan M, Mirnajafi-Zadeh J, Tiraihi T (2010) Visual evoked potentials and MBP gene expression imply endogenous myelin repair in adult rat optic nerve and chiasm following local lysolecithin induced demyelination. Brain Res 1351:50–56.

Nave KA (2010a) Myelination and support of axonal integrity by glia. Nature 468:244–252.

Nave KA (2010b) Myelination and the trophic support of long axons. Nat Rev Neurosci 11:275–283.

Neufeld AH, Gachie EN (2003) The inherent, age-dependent loss of retinal ganglion cells is related to the lifespan of the species. Neurobiol Aging 24:167–172.

Neumann B, Baror R, Zhao C, Segel M, Dietmann S, Rawji KS, Foerster S, McClain CR, Chalut K, van Wijngaarden P, Franklin RJ (2019) Metformin restores CNS remyelination capacity by rejuvenating aged stem cells. Cell Stem Cell 25:473–485.e8.

Pan S, Mayoral SR, Choi HS, Chan JR, Kheirbek MA (2020) Preservation of a remote fear memory requires new myelin formation. Nat Neurosci 23:487–499.

Patel NB, Lim M, Gajjar A, Evans KB, Harwerth RS (2014) Age-associated changes in the retinal nerve fiber layer and optic nerve head. Invest Ophthalmol Vis Sci 55:5134–5143.

Podoleanu AG (2012) Optical coherence tomography. J Microsc 247:209–219.

Rivera AD, Pieropan F, Chacon-De-La-Rocha I, Lecca D, Abbracchio MP, Azim K, Butt AM (2021) Functional genomic analyses highlight a shift in Gpr17-regulated cellular processes in oligodendrocyte progenitor cells and underlying myelin dysregulation in the aged mouse cerebrum. Aging Cell 20:e13335.

Ruckh JM, Zhao JW, Shadrach JL, van Wijngaarden P, Rao TN, Wagers AJ, Franklin RJ (2012) Rejuvenation of regeneration in the aging central nervous system. Cell Stem Cell 10:96–103.

Sadick JS, O'Dea MR, Hasel P, Dykstra T, Faustin A, Liddelow SA (2022) Astrocytes and oligodendrocytes undergo subtype-specific transcriptional changes in Alzheimer's disease. Neuron 110:1788–1805.e10.

Samuel MA, Zhang Y, Meister M, Sanes JR (2011) Age-related alterations in neurons of the mouse retina. J Neurosci 31:16033–16044.

Sandell JH, Peters A (2001) Effects of age on nerve fibers in the rhesus monkey optic nerve. J Comp Neurol 429:541–553.

Segel M, Neumann B, Hill MF, Weber IP, Viscomi C, Zhao C, Young A, Agley CC, Thompson AJ, Gonzalez GA, Sharma A, Holmqvist S, Rowitch DH, Franze K, Franklin RJ, Chalut KJ (2019) Niche stiffness underlies the ageing of central nervous system progenitor cells. Nature 573:130–134.

Simons M, Nave KA (2015) Oligodendrocytes: myelination and axonal support. Cold Spring Harb Perspect Biol 8:a020479.

Skoff RP, Price DL, Stocks A (1976) Electron microscopic autoradiographic studies of gliogenesis in rat optic nerve: II. Time of origin. J Comp Neurol 169:313–334.

Stadelmann C, Timmler S, Barrantes-Freer A, Simons M (2019) Myelin in the central nervous system: structure, function, and pathology. Physiol Rev 99:1381–1431.

Steadman PE, Xia F, Ahmed M, Mocle AJ, Penning AR, Geraghty AC, Steenland HW, Monje M, Josselyn SA, Frankl PW (2020) Disruption of oligodendrogenesis impairs memory consolidation in adult mice. Neuron 105:150–164.e6.

Sugita Y, Yamamoto H, Maeda Y, Furukawa T (2020) Influence of aging on the retina and visual motion processing for optokinetic responses in mice. Front Neurosci 14:586013.

Theelen T, Teussink MM (2018) Inspection of the human retina by optical coherence tomography. Methods Mol Biol 1715:351–358.

Tripathi RB, Jackiewicz M, McKenzie IA, Kougioumtzidou E, Grist M, Richardson WD (2017) Remarkable stability of myelinating oligodendrocytes in mice. Cell Rep 21:316–323.

Wang F, Yang YJ, Yang N, Chen XJ, Huang NX, Zhang J, Wu Y, Liu Z, Gao X, Li T, Pan GQ, Liu SB, Li HL, Fancy SP, Xiao L, Chan JR, Mei F (2018) Enhancing oligodendrocyte myelination rescues synaptic loss and improves functional recovery after chronic hypoxia. Neuron 99:689–701.e5.

Wang F, Ren SY, Chen JF, Liu K, Li RX, Li ZF, Hu B, Niu JQ, Xiao L, Chan JR, Mei F (2020) Myelin degeneration and diminished myelin renewal contribute to age-related deficits in memory. Nat Neurosci 23:481–486.

Xiao L, Ohayon D, McKenzie IA, Sinclair-Wilson A, Wright JL, Fudge AD, Emery B, Li H, Richardson WD (2016) Rapid production of new oligodendrocytes is required in the earliest stages of motor-skill learning. Nat Neurosci 19:1210–1217.

Yang SM, Michel K, Jokhi V, Nedivi E, Arlotta P (2020) Neuron class-specific responses govern adaptive myelin remodeling in the neocortex. Science 370:eabd2109.

Yeung MS, Zdunek S, Bergmann O, Bernard S, Salehpour M, Alkass K, Perl S, Tisdale J, Possnert G, Brundin L, Druid H, Frisén J (2014) Dynamics of oligodendrocyte generation and myelination in the human brain. Cell 159:766–774.

Young KM, Psachoulia K, Tripathi RB, Dunn SJ, Cossell L, Attwell D, Tohyama K, Richardson WD (2013) Oligodendrocyte dynamics in the healthy adult CNS: evidence for myelin remodeling. Neuron 77:873–885.

Yu Y, Chen Y, Kim B, Wang H, Zhao C, He X, Liu L, Liu W, Wu LM, Mao M, Chan JR, Wu J, Lu QR (2013) Olig2 targets chromatin remodelers to enhancers to initiate oligodendrocyte differentiation. Cell 152:248–261.

Zhang C, Hua T, Li G, Tang C, Sun Q, Zhou P (2008) Visual function declines during normal aging. Curr Sci 95:1544–1550.

Zhang X, Zhu J, Chen X, Jie-Qiong Z, Li X, Luo L, Huang H, Liu W, Zhou X, Yan J, Lin S, Ye J (2019) Interferon regulatory factor 3 deficiency induces age-related alterations of the retina in young and old mice. Front Cell Neurosci 13:272.

Zhou Q, Choi G, Anderson DJ (2001) The bHLH transcription factor Olig2 promotes oligodendrocyte differentiation in collaboration with Nkx2.2. Neuron 31:791–807.